Four Climate Cycles of Recurring Deep and Surface Water Destabilizations on the Iberian Margin

Belen Martrat *et al.*

Science **317**, 502 (2007);
DOI: 10.1126/science.1139994

Science (print ISSN 0036-8075; online ISSN 1095-9203) is published weekly, except the last week in December, by the American Association for the Advancement of Science, 1200 New York Avenue NW, Washington, DC 20005.

outline [fig. S9; although the rate of increase in disparity of cranidial shape was highest in the Early Cambrian and slowed from the Middle Cambrian through Middle Ordovician (figure 5 in (*6*)]. The role of intraspecific variation in the generation of novelty and therefore of macroevolutionary trends in disparity is unclear: A hypothesis that intraspecific variation is the source of disparity increase predicts that a polymorphism should involve a derived feature, but the data relate only to whether or not a species is polymorphic for a given character, irrespective of whether the character states are derived, primitive, or convergent on another species.

The observed decline in intraspecific variation may have resulted from increasing developmental or ecological constraints. Developmental constraints may stem from increased integration among or regulation of developmental systems, resulting in decreased capacity to generate or accommodate change in those systems without negative effects on viability (*4*, *28*–*33*). Ecological constraints may stem from progressive niche specialization associated with increased diversity and competition: In an ecospace dominated by incumbents, selection pressure could reduce fitness of variant phenotypes even though developmental regulation and integration may remain unchanged (*29*, *34*). Constraint resulting from a decline in developmental flexibility, in success rate for ecological establishment, or in both (*2*, *4*) could lead to loss of phenotypic variation within species and diminishing morphological innovation, which translates into slower response to selection and declining rate of morphological and taxonomic diversification. Further investigation is required to determine the causal mechanisms and whether the post-Middle Cambrian decline in the frequency and extent of intraspecific variation detected here was unique to trilobites or to this time interval. Nevertheless, demonstration of this pattern and its potential correspondence to diversification rate in trilobites suggests that within-species variation may play an important role in shaping clade macroevolutionary history.

References and Notes

1. S. J. Gould, *Wonderful Life: The Burgess Shale and the Nature of History* (Norton, New York, 1989).
2. D. Jablonski, *Palaeontology* **50**, 87 (2007).
3. M. Foote, *Annu. Rev. Ecol. Syst.* **28**, 129 (1997).
4. D. H. Erwin, *Palaeontology* **50**, 57 (2007).
5. S. J. Gould, N. L. Gilinsky, R. Z. German, *Science* **236**, 1437 (1987).
6. M. Foote, *Paleobiology* **19**, 185 (1993).
7. G. P. Wagner, L. Altenberg, *Evolution* **50**, 967 (1996).
8. P. D. Sniegowski, H. A. Murphy, *Curr. Biol.* **16**, R831 (2006).
9. V. Jaanusson, *Fossils and Strata* **4**, 209 (1975).
10. L. Ramsköld, *Trans. R. Soc. Edinb. Earth Sci.* **82**, 143 (1991).
11. J. M. Adrain, R. A. Fortey, S. R. Westrop, *Science* **280**, 1922 (1998).
12. N. C. Hughes, in *Evolving Form and Function: Fossils and Development*, D. E. G. Briggs, Ed. (Peabody Museum of Natural History, Yale Univ., New Haven, CT, 2005), pp. 139–158.
13. M. Foote, *Palaeontology* **34**, 461 (1991).
14. R. A. Fortey, R. M. Owens, in *Evolutionary Trends*, K. J. McNamara, Ed. (Belhaven, London, 1990), pp. 121–142.
15. K. J. McNamara, *Biol. Rev.* **61**, 121 (1986).
16. N. C. Hughes, *Geology* **19**, 913 (1991).
17. Materials and methods are available as supporting material on *Science* Online.
18. J. M. Adrain, *GSA Abstr. Prog.* **38**, 207 (2006).
19. R. A. Fortey, *J. Paleontol.* **75**, 1141 (2001).
20. T. J. Cotton, R. A. Fortey, in *Crustacea and Arthropod Relationships*, S. Koenemann, R. A. Jenner, Eds., vol. 16 of *Crustacean Issues* (Taylor & Francis, Boca Raton, FL, 2005), pp. 95–136.
21. E. B. Naimark, *Paleontol. J.* **40**, 541 (2006).
22. Extremely poor taxonomic representation may bias estimates of Late Cambrian intraspecific variation. Ptychopariid clades underwent a series of pronounced radiations during the Late Cambrian and accounted for most of the trilobite diversity at this time, but are grossly undersampled in the present study (only eight species represented).
23. N. C. Hughes, R. E. Chapman, J. M. Adrain, *Evol. Dev.* **1**, 24 (1999).
24. M. Foote, *Paleobiology* **14**, 258 (1988).
25. D. Schluter, *Evolution* **50**, 1766 (1996).
26. S. Renaud, J.-C. Auffray, J. Michaux, *Evolution* **60**, 1701 (2006).
27. M. J. West-Eberhard, *Developmental Plasticity and Evolution* (Oxford Univ. Press, New York, 2003).
28. R. Riedl, *Order in Living Organisms: A Systems Analysis of Evolution* (Wiley, New York, 1978).
29. J. W. Valentine, *Palaios* **10**, 190 (1995).
30. G. P. Wagner, M. D. Laubichler, *J. Exp. Zool. B Mol. Dev. Evol.* **302B**, 92 (2004).
31. G. E. Budd, *Biol. Rev.* **81**, 609 (2006).
32. E. H. Davidson, D. H. Erwin, *Science* **311**, 796 (2006).
33. Developmental regulation controlling morphogenesis of the features coded in cladistic analyses of trilobites must have lain downstream of the hypothesized kernels of gene-regulatory networks specifying body-plan architecture (*32*). Complex, phylum-defining characters are not seen to vary within species, and their long-term stability renders consideration of their evolution as "population polymorphisms writ large" inappropriate (*31*). The decline in intraspecific variation documented here is therefore unlikely to simply extrapolate into an explanation for the uniqueness of the Cambrian radiation of metazoans.
34. D. H. Erwin, *Acta Palaeontol. Pol.* **38**, 281 (1994).
35. R. Fortey, T. Cotton, S. Westrop, J. Adrain, and G. Edgecombe discussed aspects of character coding and taxonomic sampling in their cladistic analyses. A. R. Palmer assisted in determining the stratigraphic provenance of several species. Comments from D. Jablonski, M. Foote, P. Wagner, P. Crane, B. Sinclair, and two reviewers helped improve the analysis and manuscript. L. Qin translated Chinese literature. Fig. S1 was drafted by M. Foote.

Supporting Online Material

www.sciencemag.org/cgi/content/full/317/5837/499/DC1
Materials and Methods
SOM
Figs. S1 to S9
Tables S1 and S2
References

23 March 2007; accepted 6 June 2007
10.1126/science.1142964

Four Climate Cycles of Recurring Deep and Surface Water Destabilizations on the Iberian Margin

Belen Martrat,[1] Joan O. Grimalt,[1]* Nicholas J. Shackleton,[2]† Lucia de Abreu,[2] Manuel A. Hutterli,[3,4] Thomas F. Stocker[4]

Centennial climate variability over the last ice age exhibits clear bipolar behavior. High-resolution analyses of marine sediment cores from the Iberian margin trace a number of associated changes simultaneously. Proxies of sea surface temperature and water mass distribution, as well as relative biomarker content, demonstrate that this typical north-south coupling was pervasive for the cold phases of climate during the past 420,000 years. Cold episodes after relatively warm and largely ice-free periods occurred when the predominance of deep water formation changed from northern to southern sources. These results reinforce the connection between rapid climate changes at Mediterranean latitudes and century-to-millennial variability in northern and southern polar regions.

The study of abrupt climate change has focused mainly on the last glacial period (*1*–*13*) and has provided important insights about the dynamics of the climate system (*14*, *15*). Synchronization of the $\delta^{18}O$ records from Greenland and Antarctic ice cores has shown that the regions around Antarctica were warming during short-term cooling stages in Greenland (*1*). These high-latitude changes were paralleled by the fine-scale variability of sea surface temperatures (SST) from lower latitudes in their respective hemispheres (*16*, *17*) and were directly linked on a regional scale to the extension and retreat of polar ice (*3*, *4*) and the reorganization of atmospheric (*5*, *6*) and oceanic circulation (*7*–*13*).

A number of paleoarchives have shown that century-to-millennial climate variability also was

[1]Department of Environmental Chemistry, Chemical and Environmental Research Institute of Barcelona, Spanish National Research Council (IIQAB-CSIC), 08034 Barcelona, Spain. [2]Godwin Laboratory for Palaeoclimate Research, Department of Earth Sciences, University of Cambridge, Cambridge, CB2 3EQ, UK. [3]British Antarctic Survey, High Cross, Madingley Road, Cambridge, CB3 0ET, UK. [4]Climate and Environmental Physics, Physics Institute, University of Bern, CH-3012 Bern, Switzerland.

*To whom correspondence should be addressed. E-mail: jgoqam@cid.csic.es
†Deceased.

a robust feature in previous climate cycles (*16*–*25*). However, in these cases, no ice records from the Northern Hemisphere were available for a comprehensive test of the hypothesis that the same dynamics of abrupt climate change existed during previous ice ages. Fortunately, high-resolution marine sediment cores from the Iberian margin contain a record of the different water masses, which came from the northern North Atlantic and Antarctic regions. In these cores, the $\delta^{18}O$ record of benthic foraminifera resembled the Antarctic temperature signal, whereas the $\delta^{18}O$ of planktic foraminifera exhibited changes similar to those found in Greenland ice cores (*7*–*9*). The differences in isotopic composition between surface and deep waters were based on measurements along individual cores and consequently provided a first independent verification of earlier methane interhemispheric phasing for the last climate cycle (*1*).

The Iberian margin is therefore a focal point for comprehensive evaluation of climate variability in both hemispheres over long time periods. We analyzed stable isotopes (n = 1396 samples) and fossil organic compounds synthesized by marine and continental flora (n = 1648 samples) that we found in sediment cores MD01-2443 and MD01-2444; these data allowed us to generate a high-resolution reconstruction of the climatic history of the past 420,000 years (Fig. 1 and Table 1) (*26*–*28*).

Analysis of down-core profiles on their depth scales emphasizes that climatic events recorded in the incremental layers do not vary in shape after application of dating techniques (fig. S1A). The alkenone-derived SST at the Iberian margin is coupled with the $\delta^{18}O$ record of *Globigerina bulloides* (fig. S1B). The specific sedimentation features of the area studied prevent the offset between ages of alkenones and foraminifera from identical sediment depth intervals, further supporting the in-depth evaluation from the nearby northwest African margin (*29*).

None of the climate cycles was an exact reproduction of the others because on the orbital time scale the governing factors of ice-age dynamics have never been identical (*19*, *20*, *30*–*32*) (Fig. 2, A and B). The results show that the rapid SST changes (Fig. 2F) are consistent, for the time span in which they overlap, with Greenland $\delta^{18}O$ profiles (*2*), reconstructions of iceberg discharges at 55°N (*21*), and arboreal pollen in southern Europe (*22*, *23*) (Fig. 2, B to E).

Dansgaard/Oeschger-type variability is recorded all along the Iberian margin over the past four climate cycles (Fig. 2F). For simplification purposes, the warm and cool events are listed and labeled, respectively, as Iberian margin interstadials (IMI) and stadials (IMS), with the

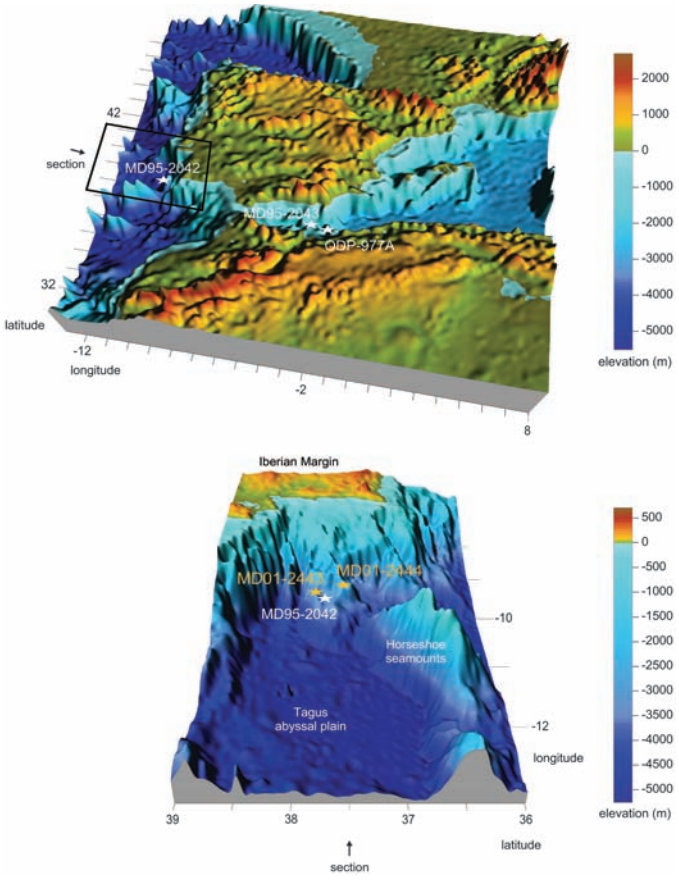

Fig. 1. Maps showing the location of the Iberian margin sediment cores (*28*). The sediment cores studied are MD01-2444 (37°33.68′N, 10°08.53′W, 2637 m below sea level) and MD01-2443 (37°52.85′N, 10°10.57′W, 2925 m below sea level). Existing relevant paleoarchives are MD95-2042 (*7*, *8*, *12*, *13*), MD95-2043 (*10*, *11*), and ODP-977A (*16*), all of which establish the Iberian margin as a sensitive region for recording climatic changes.

Table 1. Summary of the Iberian margin alkenone unsaturation index ($U^{k'}_{37}$)—SST (°C) conditions and time resolution (years) in cores MD01-2444 and MD01-2443 over the past four climate cycles. The average temporal resolution remains comparable at centennial scale throughout the entire period studied. Cores MD01-2444, ODP-977A (*16*), and MD95-2042 (*12*) are in close agreement over the first climate cycle. Correlation coefficients of ODP-977A (*16*) and MD01-2444 $U^{k'}_{37}$-SST (°C) with NGRIP $\delta^{18}O$ (*2*) are r = 0.88 and r = 0.86, respectively. The correlation coefficient of the MD01-2443 benthic profile [(*26*, *27*) and this study] with the Dome C δD record (*18*) is r = 0.92.

SST (°C) μ ± σ [time resolution (years) μ ± σ]	First climate cycle		Second climate cycle		Third climate cycle		Fourth climate cycle	
	Glacial	Interglacial	Glacial	Interglacial	Glacial	Interglacial	Glacial	Interglacial
MD01-2444, n = 902 samples (this study)	13.8 ± 1.1	17.3 ± 1.9	13.9 ± 2.0					
	[136 ± 83]	[275 ± 124]	[321 ± 255]					
MD01-2443, n = 764 samples (this study)			14.6 ± 1.3	17.9 ± 1.4	12.6 ± 2.5	16.8 ± 1.8	12.3 ± 2.2	17.2 ± 1.3
			[590 ± 412]	[428 ± 250]	[388 ± 144]	[333 ± 197]	[584 ± 371]	[250 ± 149]
ODP-977A, n = 655 samples (*16*)	13.1 ± 1.7	17.9 ± 3.0	14.1 ± 2.2	18.0 ± 2.6				
	[317 ± 234]	[448 ± 522]	[370 ± 180]	[378 ± 233]				
MD95-2042, n = 299 samples (*12*)	14.5 ± 1.4	17.6 ± 2.2						
	[358 ± 199]	[923 ± 344]						

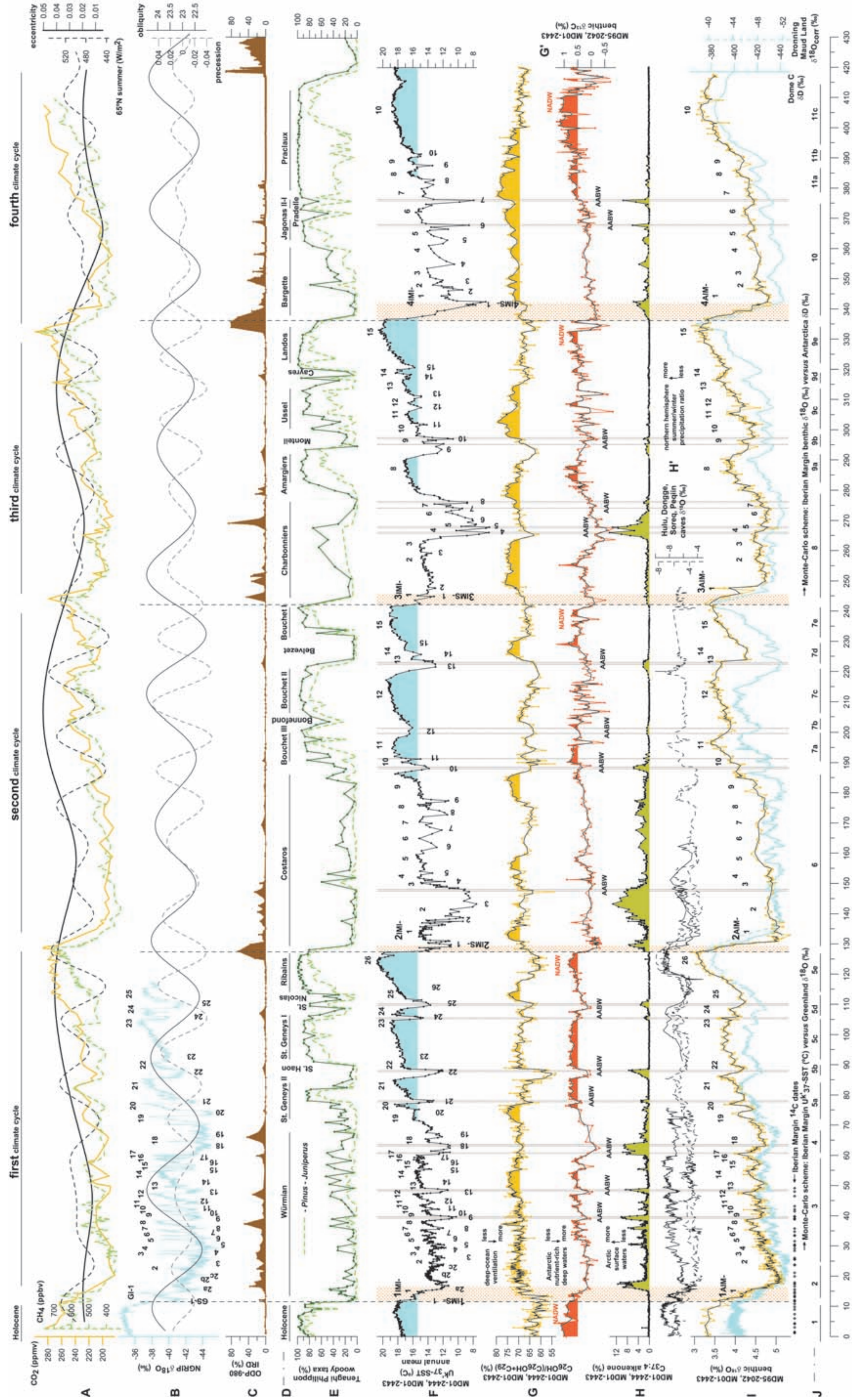
Holocene
first climate cycle
second climate cycle
third climate cycle
fourth climate cycle
age (calendar ky before the present)
Monte-Carlo scheme: Iberian Margin benthic δ18O (‰) versus Antarctica δD (‰)
Iberian Margin 14C dates
Monte-Carlo scheme: Iberian Margin UK'37-SST (°C) versus Greenland δ18O (‰)
Würmian
Costaros
Charbonniers
Amargiers
Ussel
Landos
Bargette
Praclaux
Ribains
NADW
AABW

Fig. 2. Comparison between the Iberian margin paleoarchive and distance records over the last four interglacial-to-glacial cycles. (**A**) The greenhouse gases CO_2 [solid yellow curve, in parts per million by volume (ppmv)] and CH_4 [dashed green curve, in parts per billion by volume (ppbv)] (*19*, *20*), the eccentricity of the Earth's orbit (solid black curve), and the daily insolation at 65°N during the summer solstice (dashed black curve). These data, along with (**B**) phasing in Earth's obliquity (solid black curve) and precession (dashed gray curve) (*30*) are external triggers of the climate system, although a substantially nonlinear response to these gradual forcings (*31*, *32*) also is evident in the profiles presented here. The North Greenland Ice Core Project (NGRIP) $\delta^{18}O$ profile [per mil (‰)] (*2*) is drawn with the isotopically defined Greenland interstadials (GI) on the top and the subsequent Greenland stadials (GS) on the bottom. (**C**) The ODP-980 relative proportion of detrital lithics ice-rafted debris (IRD) record events when the ice shelves reached a critical extension (*21*). (**D**) The Velay pollen sequence stratigraphy (*23*) applied to (**E**) the Tenaghi Philippon woody taxa; the pollen curve excluding *Pinus* and *Juniperus* is shown by the dashed line, because the ecological requirements of these two genera are not always indicative of temperate climates (*22*). (**F**) $U^{k'}_{37}$-SST in a composite of cores MD01-2444 and MD01-2443 with the IMI on the top and the IMS on the bottom, with the number of the climate cycle to which they belong shown immediately before (values above average are shaded blue). Areas shaded orange show transitions between the climate cycles, and gray areas mark the most prominent bifurcations in climate conditions. (**G**) The relative proportion of *n*-hexacosan-1-ol ($C_{26}OH$) to the sum of *n*-hexacosan-1-ol ($C_{26}OH$) plus *n*-nonacosane (C_{29}) in cores MD01-2444 and MD01-2443 is providing an oxygenation marker of deep sea floor (three-point running average; values above average are shaded orange). (**G′**) Benthic $\delta^{13}C$ in cores MD95-2042 and MD01-2443 [data are from (*7*) and this study; three-point running average)], with alternating influence of NADW (~1 per mil) and AABW (less than 0.5 per mil). (**H**) The percentage of heptatriatetraenone ($C_{37:4}$) to total alkenones is indicative of Arctic surface waters at core locations. (**H′**) $\delta^{18}O$ of stalagmites from Hulu and Dongge caves (solid black curve) and from Soreq and Peqiin caves (dashed black curve) (*6*, *24*, *25*). (**I**) The benthic $\delta^{18}O$ profiles (solid black curve) in cores MD95-2042 and MD01-2443 [data from this study and (*7, 26, 27*)] and the Antarctic Dome C δD record (solid blue curve) (*18*) and Dronning Maud Land $\delta^{18}O$ corrected profile (dashed blue curve) (*36*), with a tentative proposal of the Antarctic isotope maxima (AIM) drawn on the top of the benthic profile. Misalignments between the Antarctic ice signal (blue curve) and the Iberian margin benthic record (yellow curve) are due to differences in the age models used, but the resemblance between the signals is unambiguous (Table 1) (*28*). (**J**) Glacial (2 to 4, 6, 8, and 10) and interglacial (1, 5, 7, 9, and 11) marine isotope stages (MISs). It should be emphasized that no ice records from the Northern Hemisphere are available for climate cycles before the last one. Greenland represents the guide for the past 120,000 years (*2*), and Antarctica is the reference for the time preceding that period (*18*). Original data and a comprehensive explanation about age scales are available online (*28*). ky, 1000 years.

number of the climate cycle to which they belong shown immediately before (e.g., 4IMS-7 is the seventh cooling stage of limited duration within the fourth climate cycle). Designation by climate cycles (interglacial followed by a glacial period) is justified on the grounds that attempting rigorous definition of the boundaries of marine isotope stages (MISs) (Fig. 2J) becomes meaningless at the centennial level (*33*).

The climate cycles commence with a rapid warming completing the deglaciation, which lasts just a few centuries (1IMS-1, 1IMS-2a, 2IMS-1, 3IMS-1, and 4IMS-1; Fig. 2F, areas shaded in orange), followed by a gradual cooling over several thousand years, often ending in a final rapid cooling phase. During the initial part of the climate cycles, warm stable periods similar to the Holocene were maintained and oscillations were rare but generally more pronounced than during the ice ages: At least four intense events interrupted the last climate period (1IMS-21, 1IMS-22, 1IMS-24, and 1IMS-25); three severe oscillations punctuated the second cycle (2IMS-11, 2IMS-12, 2IMS-13); just two interrupted the third (3IMS-9 and 3IMS-10); and none occurred during the fourth climate cycle, until sudden entry into a glacial in a single event (4IMS-7).

During fully developed glacials, the frequency of rapid climate variability also differed between climate cycles (Fig. 2F). The Iberian cores register 18 events during the first climate cycle (1IMI and 1IMS events 1 to 18), nine in the second (2IMI and 2IMS events 1 to 9), seven oscillations during the third (3IMI and 3IMS events 1 to 7), and six over the fourth (4IMI and 4IMS events 1 to 6). As a whole, there is a common general trend over the past four climate cycles: Both in variable glacials and in the warm, stable, preceding periods, the pace of climate variability increases as the Pleistocene progresses to the present. The recurring saw-tooth shape of SST fluctuations observed (Fig. 2F) points to a nonlinear threshold behavior of multiple equilibria in the North Atlantic, as referred to in models (*34*, *35*). Whatever mechanisms were responsible, the combination of triggers, amplifiers, and sources of persistence during each climate cycle was never identical, and the abundance, length, and magnitude of the events varied accordingly. For example, the last ice age was characterized by abundant multicentennial shifts, but cold spells were equally or even more severe in the three previous climate cycles (Table 1). The fourth climate cycle was the period with rapid events of the highest amplitude, but with a shorter glacial period.

In this study, we considered different hydrological indicators that permit a better link to other climate archives. First, the relative proportion of tetraunsaturated C_{37} alkenone to total C_{37} alkenones ($C_{37:4}$) is indicative of very cold surface waters at core locations (*16*). Increases in this proxy (Fig. 2H) are in line with weakening of surface Patagonian winds at specific times (*18*) and a decreasing ratio of summer-to-winter precipitation in the eastern Mediterranean and China (*6*, *24*, *25*) (Fig. 2H′). Second, the benthic $\delta^{18}O$ record of cores MD95-2042 (*7*, *8*) and MD01-2443 [see (*26*, *27*) and our data] is consistent with the profiles in Antarctica (*18*, *36*) (Fig. 2I). This correspondence supports the above analogy for the last glacial (*7*–*9*), but our results show that the correlation was maintained over the last four climate cycles. Third, the relative proportion of *n*-hexacosan-1-ol ($C_{26}OH$) to the sum of $C_{26}OH$ plus *n*-nonacosane (C_{29}) is a chemical proxy reflecting oxygenation associated with bottom current intensity, given that both compounds have the same origin (i.e., vascular terrestrial plants) but differed in resistance to degradation by oxygenation of the deep sea floor (*11*) (Fig. 2G). High and low percentages of the $C_{26}OH$ ratio [i.e., $C_{26}OH/(C_{26}OH + C_{29})$] correspond, respectively, to low and high deep-ocean ventilation. Finally, the benthic $\delta^{13}C$ record reflects the influence of both hemispheres (Fig. 2G′). Typical values of North Atlantic deep water (NADW) and Antarctic bottom water (AABW) are about 1.1 and 0.5 per mil, respectively (*37*). This indicator showed depleted values documenting entrances of AABW in the North Atlantic not only during glacials (*9*, *38*), but within the short-term cooling stages of interglacials (*21*). The common trend in changes of SST, $C_{26}OH$ ratio, and benthic $\delta^{13}C$ constitutes a recurring pattern of changes in surface and deep waters measured in the same cores. The observed time sequences of events are therefore independent of the absolute age model of choice (*28*).

Decreases in the $C_{26}OH$ ratio over the deglaciations trace the early arrival of NADW from northern latitudes. During the warmest and largely ice-free portions of the interglacials, the benthic $\delta^{13}C$ record exhibits high values for nutrient-depleted waters arriving from northern locations. Particularly during MIS 1, MIS 5e, and MIS 11c (Fig. 2J), maintenance of low $C_{26}OH$ ratio and high benthic $\delta^{13}C$ indicates conditions of high deep-water ventilation by NADW. For time intervals of 10,000 to 20,000 years after the deglaciation, the relative content of $C_{26}OH$ remained low, whereas benthic $\delta^{13}C$ and $\delta^{18}O$ values stayed high. These climate conditions evolved toward well-defined increases in the $C_{26}OH$ ratio, recording lower oxygenation and a slowdown in the intensity of bottom currents. These periods ended abruptly in harsh drops in SST preceded by steep decreases in both $C_{26}OH$ and benthic $\delta^{13}C$ ratios, indicating a reinvigoration of the deep currents, in this case caused by the inflow of southern-sourced deep waters (AABW). After the swift cold spell within a few centuries, a sharp movement back to warm SST was marked by sudden decreases in

deep water ventilation (increase in C_{26}OH ratio) and a restraint in AABW flow (increase in benthic $\delta^{13}C$).

This pattern was repeatedly observed during numerous prominent SST oscillations over the last climate cycle (1IMS-9, 1IMS-13, 1IMS-18, 1IMS-21, 1IMS-22, 1IMS-24, and 1IMS-25) (Fig. 3). This type of abrupt cooling was also pervasive during the second (2IMS-3, 2IMS-10, 2IMS-12, and 2IMS-13), the third (3IMS-4, 3IMS-5, 3IMS-7, 3IMS-8, 3IMS-9, and 3IMS-10), and the fourth climate cycle (4IMS-6 and 4IMS-7) (Fig. 2, F to I, areas shaded in gray), and it collapsed the entire Mediterranean ecosystem (*16*, *22*) parallel to a massive increase in the size of the northern ice caps (*39*). Vegetational indicators measured along MD01-2443 sediments indicate that the woodland population at the Iberian peninsula was almost nonexistent during some of these intervals, independent of glacial ice (*26*).

During MIS 10, the interhemispheric decoupling was particularly pronounced. Repeated surface temperature shifts occurred at the Iberian margin (4IMI and 4IMS events 1 to 6) and percentages of woody taxa in southern Europe were maintained at high values for almost the entire ice age (up to 78%) (*22*), but the climate variability of southern polar latitudes was almost insignificant (*18*) (Fig. 2, E to I). It is quite likely that each interstadial in northern latitudes had its counterpart in southern latitudes, but the intensity of expression in southern latitudes may vary depending on the power and duration of the event (*34*). This is consistent with the recent observation that, for the last ice age, the duration of the Greenland interstadials is correlated with the warming amplitude in Antarctica (*36*).

The changes observed point to intensification of AABW flow at the Iberian margin preceding the harsh drops in SST that characterize these rapid events (Fig. 3). The results corroborate the North Atlantic determinations of benthic $\delta^{13}C$ (*40*) or $^{231}Pa/^{230}Th$ (*41*), indicating that production of NADW decreased, and in doing so kept pace with the extension of northern polar inland glaciers to the continental shelves; however, this occurred a few centuries before the subsequent generation of icebergs. Climate scenarios that force a change in the ocean circulation with the use of a coupled ocean-atmosphere-sea ice model show that decreases in formation of NADW are capable of triggering large ice surges (*42*).

Computer simulations indicate that the imbalances between northern- and southern-sourced water masses are the primary agent for these abrupt climate oscillations (*43*). Some models propose that the interplay between these two water masses may be driven by changes in AABW (*44*, *45*) and others by NADW (*15*, *46*). However, irrespective of the ultimate origin of these deep water changes, the results presented here show that century-to-millennial variability

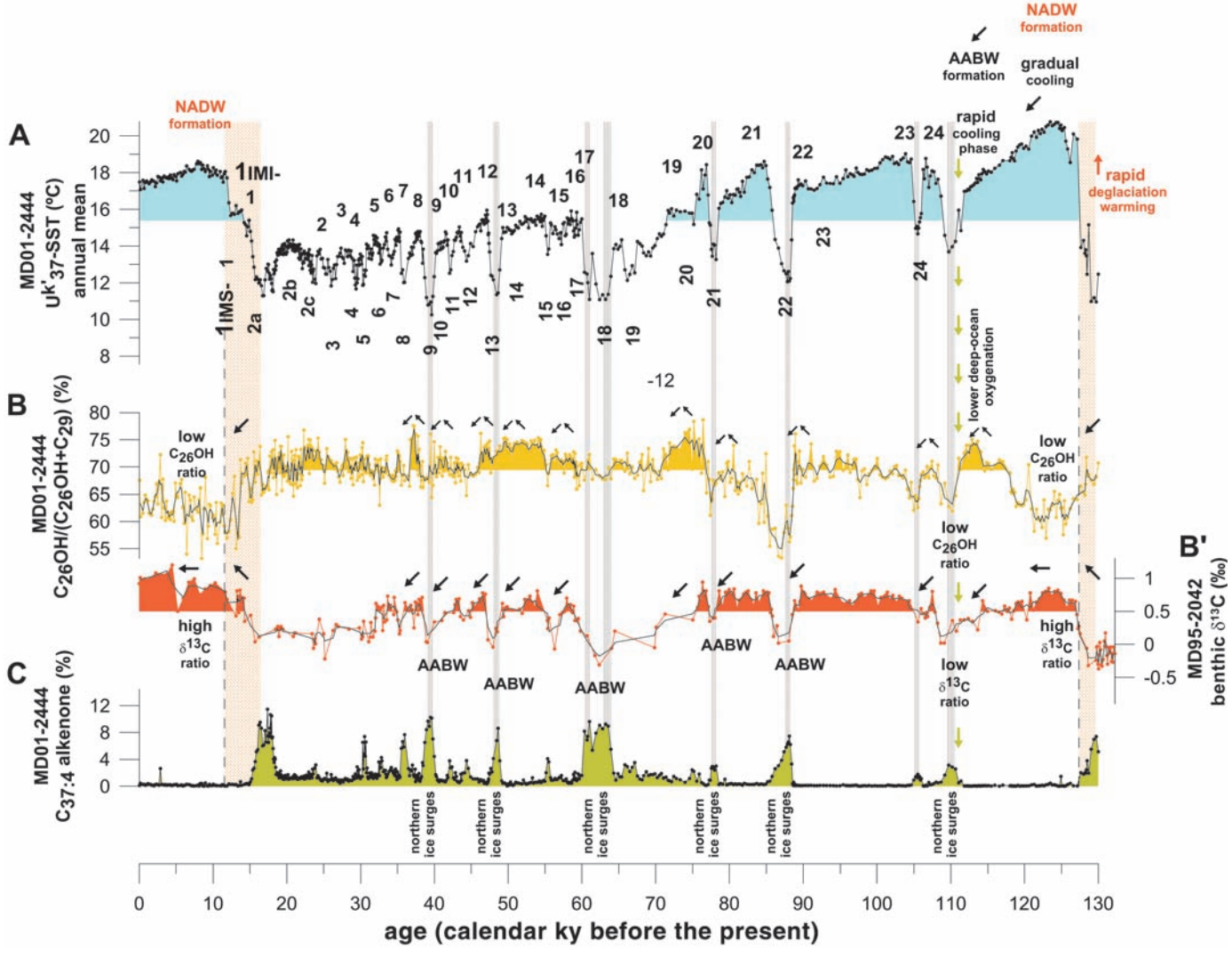

Fig. 3. A more detailed view of the time sequences of events over the last climate cycle. Harsh drops in (**A**) $U^{k'}_{37}$-SST were preceded by steep decreases in both (**B**) C_{26}OH and (**B'**) benthic $\delta^{13}C$ ratios (*7*). Hence, cold episodes after relatively warm and largely ice-free periods occurred when the predominance changed from northern deep waters (NADW) to southern (AABW). These changes occurred a few centuries before the subsequent generation of icebergs, which are traced by increases in (**C**) the percentage of $C_{37:4}$, indicative of very cold surface waters at the Iberian margin (*16*).

characteristic of the last ice age was pervasive during the entire past 420,000 years. In particular, the rapid coolings were preceded by changes in deep waters involving pulses of increasing AABW after retreat of NADW.

The finding that SST shifts become more abundant as climate cycles approach the present calls for a pressing need to understand the mechanisms of rapid climate change. The mean ~1500-year time spacing of the events of the last glacial (*47*) is not observed in previous climate cycles. This is a further indication that a time scale of this nature is not a universal characteristic of the climate system. The marked melting of the ice armadas similar to those reported over the last glacial period can no longer be uniquely associated to the cause of abrupt climate change, given that changes occurred even after relatively warm and largely ice-free periods (e.g., 1IMS-21, 1IMS-22, 3IMS-10, and others; Fig. 2F). Although more continuous freshwater discharge may not leave a notable trace in the marine sediments, it may effectively trigger the gradual deterioration of climate by slowly pushing the ocean circulation in the North Atlantic toward a threshold (*48*).

References and Notes

1. T. Blunier, E. J. Brook, *Science* **291**, 109 (2001).
2. North Greenland Ice Core Project members, *Nature* **431**, 147 (2004).
3. G. C. Bond *et al.*, *Nature* **365**, 143 (1993).
4. S. L. Kanfoush *et al.*, *Science* **288**, 1815 (2000).
5. J. R. M. Allen *et al.*, *Nature* **400**, 740 (1999).
6. Y. J. Wang *et al.*, *Science* **294**, 2345 (2001).
7. N. J. Shackleton, M. A. Hall, E. Vincent, *Paleoceanography* **15**, 565 (2000).
8. N. J. Shackleton, R. G. Fairbanks, T. Chiu, F. Parrenin, *Quat. Sci. Rev.* **23**, 1513 (2004); correction: N. J. Shackleton, *Geophys. Res. Abstr.* **7**, 1607-7962/gra/EGU05-A-05213 (2005).
9. L. C. Skinner, H. Elderfield, *Paleoceanography* **22**, PA1205 (2007).
10. I. Cacho *et al.*, *Paleoceanography* **14**, 698 (1999).
11. I. Cacho, J. O. Grimalt, F. J. Sierro, N. J. Shackleton, M. Canals, *Earth Planet. Sci. Lett.* **183**, 417 (2000).
12. D. Pailler, E. Bard, *Palaeogeogr. Palaeoclimatol. Palaeoecol.* **181**, 431 (2002).
13. E. Bard, F. Rostek, G. Ménot-Combes, *Quat. Res.* **61**, 204 (2004).
14. R. B. Alley *et al.*, *Science* **299**, 2005 (2003).
15. T. F. Stocker, S. J. Johnsen, *Paleoceanography* **18**, PA1087 (2003); correction: T. F. Stocker, S. J. Johnsen, *Paleoceanography* **20**, PA1002 (2005).
16. B. Martrat *et al.*, *Science* **306**, 1762 (2004).
17. K. Pahnke, R. Zahn, *Science* **307**, 1741 (2005).
18. EPICA community members, *Nature* **429**, 623 (2004).
19. M. Delmotte *et al.*, *J. Geophys. Res.* **109**, D12104 (2004).
20. U. Siegenthaler *et al.*, *Science* **310**, 1313 (2005).
21. J. F. McManus, D. W. Oppo, J. L. Cullen, *Science* **283**, 971 (1999).
22. P. C. Tzedakis, J. F. McManus, H. Hooghiemstra, D. W. Oppo, T. A. Wijmstra, *Earth Planet. Sci. Lett.* **212**, 197 (2003).
23. R. Cheddadi *et al.*, *Proc. Natl. Acad. Sci. U.S.A.* **102**, 13939 (2005).
24. M. Bar-Matthews, A. Ayalon, M. Gilmour, A. Matthews, C. J. Hawkesworth, *Geochim. Cosmochim. Acta* **67**, 3181 (2003).
25. D. Yuan *et al.*, *Science* **304**, 575 (2004).
26. P. C. Tzedakis, K. H. Roucoux, L. de Abreu, N. J. Shackleton, *Science* **306**, 2231 (2004).
27. L. de Abreu *et al.*, *Paleoceanography* **20**, PA3009 (2005).
28. Materials and methods are available as supporting material on *Science* Online.
29. G. Mollenhauer *et al.*, *Paleoceanography* **20**, PA1016 (2005).
30. A. L. Berger, *J. Atmos. Sci.* **35**, 2362 (1978).
31. F. Parrenin, D. Paillard, *Earth Planet. Sci. Lett.* **214**, 243 (2003).
32. P. Huybers, W. B. Curry, *Nature* **441**, 329 (2006).
33. L. C. Skinner, N. J. Shackleton, *Quat. Sci. Rev.* **24**, 571 (2005).
34. T. F. Stocker, O. Marchal, *Proc. Natl. Acad. Sci. U.S.A.* **97**, 1362 (2000).
35. M. Siddall *et al.*, *Quat. Sci. Rev.* **25**, 3185 (2006).
36. EPICA community members, *Nature* **444**, 195 (2006).
37. J. F. Adkins, A. P. Ingersoll, C. Pasquero, *Quat. Sci. Rev.* **24**, 581 (2005).
38. J. C. Duplessy *et al.*, *Paleoceanography* **3**, 343 (1988).
39. J. Mangerud *et al.*, *Quat. Sci. Rev.* **23**, 1313 (2004).
40. R. Zahn *et al.*, *Paleoceanography* **12**, 696 (1997).
41. J. F. McManus, R. François, J. M. Gherardi, L. D. Keigwin, S. Brown-Leger, *Nature* **428**, 834 (2004).
42. J. Flückiger, R. Knutti, J. W. C. White, *Paleoceanography* **21**, PA2014 (2006).
43. T. F. Stocker, D. G. Wright, W. S. Broecker, *Paleoceanography* **7**, 529 (1992).
44. J. R. Toggweiler, B. Samuels, *Deep-Sea Res.* **42**, 477 (1995).
45. G. Knorr, G. Lohmann, *Nature* **424**, 532 (2003).
46. R. Knutti, J. Flückiger, T. F. Stocker, A. Timmermann, *Nature* **430**, 851 (2004).
47. G. C. Bond *et al.*, *Science* **278**, 1257 (1997).
48. T. F. Stocker, D. G. Wright, *Nature* **351**, 729 (1991).

49. We thank P. C. Tzedakis for pollen data from Tenaghi Philippon and MD01-2443; J. Schwander for providing the Monte-Carlo wiggle-matching program; J. F. McManus for data of core ODP-980; G. C. Bond for data of core DSDP-609; E. Bard and I. Cacho for biomarker data of cores MD95-2042 and MD95-2043, respectively; North Greenland Ice Core Project members and European Project for Ice Coring in Antarctica (EPICA) community members for data of ice cores; D. Amblas for Fig. 1.; B. H. Oldham for editing the text; I. N. McCave for locating the coring sites; M. A. Hall, B. Luengo, and R. Mas for laboratory assistance; and L. C. Skinner, J. Villanueva, and W. H. Berger for providing useful comments. B.M. thanks the grant I3P-BPG2005 from the Itinerario Integrado de Inserción profesional program of the Spanish National Research Council (CSIC), and L.A. thanks the Portuguese Foundation for Science and Technology (SFRH/BPD/1588/2000). We thank the British ocean sediment core repository (BOSCOR); the International Marine Global Change Studies program (IMAGES), and the Bremen core repository [Ocean Drilling program (ODP)] for supplying sediment samples. This work was supported by the Pole-Ocean-Pole (EVK2-2000-00089) and Patterns of Climate Variability in the North Atlantic (EVR1-2002-000413) projects funded by the European Union.

Supporting Online Material

www.sciencemag.org/cgi/content/full/1139994/DC1
Materials and Methods
Fig. S1
References
Original Data File

16 January 2007; accepted 4 June 2007
Published online 14 June 2007;
10.1126/science.1139994
Include this information when citing this paper.

Ethylene Modulates Stem Cell Division in the *Arabidopsis thaliana* Root

Olga Ortega-Martínez,*† Monica Pernas,*‡ Rachel J. Carol, Liam Dolan§

The construction of multicellular organisms depends on stem cells—cells that can both regenerate and produce daughter cells that undergo differentiation. Here, we show that the gaseous messenger ethylene modulates cell division in the cells of the quiescent center, which act as a source of stem cells in the seedling root. The cells formed through these ethylene-induced divisions express quiescent center-specific genes and can repress differentiation of surrounding initial cells, showing that quiescence is not required for these cells to signal to adjacent stem cells. We propose that ethylene is part of a signaling pathway that modulates cell division in the quiescent center in the stem cell niche during the postembryonic development of the root system.

The bodies of multicellular land plants are derived from populations of dividing cells called meristems, which contain stem cells. Clonal analysis revealed that the ultimate source of cells in the *Arabidopsis thaliana* root meristem is the quiescent center (QC), a group of four cells that divides infrequently and can give rise to cells in all tissue systems of the root (*1*). The QC cells are surrounded by initials that divide to regenerate themselves and produce cells that contribute to the root body and have also been considered to be stem cells (*2*, *3*). Because initials can be replaced by QC cells, the former may be considered to be short-term stem cells, whereas the latter are long-term stem cells. QC cells produce signals that promote division of the abutting initial cells and repress initial cell terminal differentiation (*4*). Together, the QC cells and the surrounding initial cells constitute a stem cell niche (*5*, *6*).

To identify genes that control cell proliferation in the stem cell niche, we screened our collection of root mutants for plants with defective QC cellular organization resulting from deregulated QC cell division. We identified two mutants, E6263 and E4510, in which the cells of the QC divide (Fig. 1, B to F). In the E6263 mutant

Department of Cell and Developmental Biology, John Innes Centre, Norwich NR4 7UH, UK.

*These authors contributed equally to this work.
†Present address: Kristineberg Marine Research Station, Kristineberg 566, 450 34 Fiskebäckskil, Sweden.
‡École Pratique des Hautes Études, 46 rue de Lille, 75007 Paris, France.
§To whom correspondence should be addressed. E-mail: liam.dolan@bbsrc.ac.uk